Absorption, luminescence and scattering of single nano-objects

Yorulmaz, M.

CHAPTER 4

Correlated absorption and photoluminescence of single gold nanospheres

We perform simultaneous absorption (photothermal) and fluorescence detection of gold nanospheres with diameters of 80, 60, 40, 20, 10, and 5 nm. We unambiguously identify the same individual nanoparticles (NPs) over large areas (>400 μm^2) by means of atomic force microscopy (AFM) and optical absorption (photothermal) microscopy. We correlate the height of NPs measured with AFM with absorption and fluorescence signals from the same individual NPs. That allows us to compare their brightness and estimate their fluorescence quantum yield at the single NP level. We also demonstrate a laser-induced enhancement of luminescence of 20 nm gold nanospheres. Simultaneous absorption and fluorescence detection of gold nanospheres makes them attractive for biosensing and multidimensional tracking applications where durable and nontoxic labels and complementary signals are required.

The contents of this chapter are based on:
A. Gaiduk, M. Yorulmaz, and M. Orrit, "Correlated absorption and photoluminescence of single gold nanoparticles", ChemPhysChem **12**, 1536-1541 (2011) and A. Gaiduk, P. Ruijgrok, M. Yorulmaz, and M. Orrit, "Making gold nanoparticles fluorescent for simultaneous absorption and fluorescence detection on the single particle level", Phys. Chem. Chem. Phys. **13**, 149-153 (2011)

4.1 Introduction

Gold nanoparticles (NPs) of various sizes and shapes, and with different surface properties, are commonly used as labels for optical microscopy.[133,134,174,175] These labels can be detected individually either by their scattering, absorption, or photoluminescence.[23,38,40–42,75,87,91,149,150,176–179] Although the quantum efficiency of the photoluminescence of gold NPs is very low, their large absorption cross section makes them detectable, opening possible applications. Earlier efforts to measure and understand the emission of gold NPs have rested on ensemble measurements on NPs of various sizes and shapes. A photoluminescence efficiency of 10^{-6} was reported for $4 - 80$ nm (diameter) spherical NPs in water.[180] Different theoretical descriptions have been proposed to understand the emission of AuNPs.[180–182] In essence, the electron-hole pairs created by optical excitation rapidly relax towards the Fermi sea level, but can still recombine radiatively with a low probability. Coupling of electrons and holes to the collective plasmon modes of a NP can enhance their radiative recombination rate and explain that the luminescence spectrum of gold NPs displays the same plasmonic resonances appearing in their absorption spectrum. Dulkeith et al.[180] have argued that, in the dipole approximation, the radiative coupling scales as the volume of the particle, whereas the screening factor effect reducing coupling of individual charges to plasmon modes scales as the inverse of the volume. The combination of these two effects explains the experimental observation that the quantum yield of gold NPs does not significantly depend on size for diameters between 5 and 50 nm, for which the dipole approximation applies. More recently, it has been shown that the presence of an imbedding/stabilizing medium and surface modification can influence the observed fluorescence signals.[155,183–186].

Photothermal microscopy is one of the methods allowing background-free detection of absorbers at room temperature,[38,39,90,95,97,98,187,188] with a sensitivity reaching the single-molecule level (see Chapter 2).[82] Further developments of this technique, including photothermal correlation spectroscopy,[124,189,190] photothermal tracking,[28] wide-field photothermal detection,[191] and its combination with fluorescence microscopy make photothermal microscopy a valuable tool in a large variety of applications. In this work, we simultaneously detected absorption and luminescence signals from the same single spherical gold NPs, which allows us to estimate directly their lu-

minescence quantum yield.[155] We also checked the sizes of these same NPs by correlating their optical images with atomic force microscopy (AFM) images. We used commercial gold NPs of various diameters providing both absorption (photothermal) and fluorescence signals. We compare their photoluminescence quantum yield to previously reported results from ensemble experiments. We also show, in a separate experiment, a laser-induced enhancement of luminescence of 20 nm diameter gold NPs. We conclude that individual small gold NPs with diameters as small as 5 nm could serve as nonbleaching labels for luminescence detection and tracking, and shortly discuss further perspectives of simultaneous photothermal and fluorescence detection of single gold NPs of various shapes.

4.2 Experimental section

4.2.1 Absorption (photothermal) and fluorescence microscopy

The absorption of individual NPs was measured by photothermal contrast. Photothermal detection is described in detail in Chapter 2. The experimental setup for simultaneous absorption and fluorescence microscopy was home-built around an inverted optical microscope, Olympus IX71, equipped with an Olympus 60× oil immersion objective (NA=1.45) and the simultaneous absorption and luminescence detection was performed as described in Chapter 3.

Briefly, correlated absorption and luminescence signals were detected while nanospheres with diameters of 80, 60, 40, 20, 10, and 5 nm were excited by the heating beam at 514 nm which was provided by an Ar-Ion laser (Coherent Innova 300) and modulated at a frequency of 740 kHz. The dissipated energy gives rise to a time-dependent temperature gradient around the nano-absorber. The maximum temperature rise in steady state on the surface of the particle is, $\Delta T = \frac{\sigma_{abs} I_{heat}}{4\pi\kappa R}$ where σ_{abs} is the absorption cross section of the NP, I_{heat} is the intensity (irradiance) of the heating laser, κ is the thermal conductivity of the medium around the NP, and R is its radius.

For photothermal detection, the probe beam was produced by a Ti:sapphire laser (S3900 s, Spectra Physics) which operated at 800 nm for this experiment. The small change in the detected probe intensity due to photothermal effect was isolated by using a lock-in amplifier to provide the

photothermal signal.

The luminescence detection was performed in the backward direction by spectral separation of the luminescence signal at the dichroic mirror (AHF z532/NIR). The luminescence signal was additionally spatially filtered by a 50 μm confocal pinhole and spectrally filtered by a set of bandpass filters (AHF 615/150 and Omega 595/100) and detected by an avalanche photon-counting module (SPCM-AQR-16).

In an independent experiment, we study a laser-induced method to enhance the luminescence signal of 20 nm diameter gold nanospheres. For the initial investigation of the observed luminescence enhancement, 532 nm laser light (Shangi Lasers) was used as the heating beam and the intensity of the laser was modulated at 740 kHz. 790 nm laser light (Mira, Coherent) was employed as the probe beam. For luminescence imaging, the heating beam was sent to the back-aperture of the microscope objective after it was reflected off from a 30/70 (Reflection/Transmission) beamsplitter. The back-reflected signal collected by the same microscope objective was sent through the same 30/70 beamsplitter. Then, the luminescence of 20 nm diameter gold nanospheres was spectrally selected by a set of bandpass filers (AHF 615/150 and Omega 595/100) and directly detected by an avalanche photon counting module (SPCM-AQR-16). There was no pinhole in the fluorescence detection path to suppress fluorescence background from out-of-focus planes. Moreover, the background signals of luminescence images was higher than the background signal of the images obtained by using the former described setup. Therefore, the intrinsic luminescence of gold nanospheres was not detectable in this case.

4.2.2 Atomic force microscopy (AFM)

We used an atomic force microscope (Digital Instruments) in tapping mode equipped with cantilevers with a resonance frequency of 280 kHz. We recorded AFM images in air to characterize the topography of our samples.

4.2.3 Sample preparation

Samples of colloidal suspensions of gold NPs with diameters of 80, 60, 50, 40, 30, 20, 10, and 5 nm (British Biocell International) were prepared by dilution in ultra-pure water at volume ratios of 1:1, 1:4, 1:4, 1:8, 1:20, 1:20, 1:150, and

1:1000, respectively. Approximately 50 μL of the suspension were deposited on the surface of cleaned glass immediately after filtration through a 450 nm porous membrane (except for the 80 nm diameter NPs) and spin-coated at 2000 rpm for 5 s, followed by drying at 4000 rpm for 90 s.

Glass coverslides (Menzel, Germany) were cleaned in several steps by sonication for 20 min, successively in a Hellmanex (Hellma) solution in water (2%), in acetone, in ethanol (both 96%purity), and in Milli-Q water after each cleaning step. The surfaces were modified with 3-aminopropylthriethylethoxysilane (APTES, Sigma-Aldrich) by immersing clean coverslides in APTES solution in acetone (2%) overnight. Experiments were performed in a fluid cell (approx. $50 - 150$ μL volume). We used glycerol (>99.5%, spectrophotometric grade) as the photothermal transducing fluid in all experiments. The background fluorescence of glycerol was too high to detect the luminescence of the smaller gold beads (5 nm). Their luminescence and photothermal signals were measured in air and calibrated with those of larger NPs (20 nm) under the same conditions.

4.3 Results and discussion

4.3.1 AFM characterization of gold NPs

The results of our AFM studies of commercial spherical gold NPs of various sizes are shown in Fig. 4.1 and Table 4.1. The mean values of measured heights are in good agreement with the specified diameters. The spreads of heights for individual NPs of 20, 40, 50, 60, and 80 nm diameter are about 11% (rms), which is close to 8-10 percent specification values. However, larger variations are observed for NPs with nominal diameters of 5, 10, and 30 nm. In particular, for the NPs with specified diameter of 30 nm a distinct population of smaller NPs leads to a 19% variation of the measured height. The differences between the actual mean values and the nominal diameters can be explained by the nonspherical shapes of the NPs. Because our AFM images were recorded at a relatively low resolution over large sample areas in order to correlate them with optical images, they did not allow us to retrieve the detailed nonspherical shape of NPs in the present experiments.

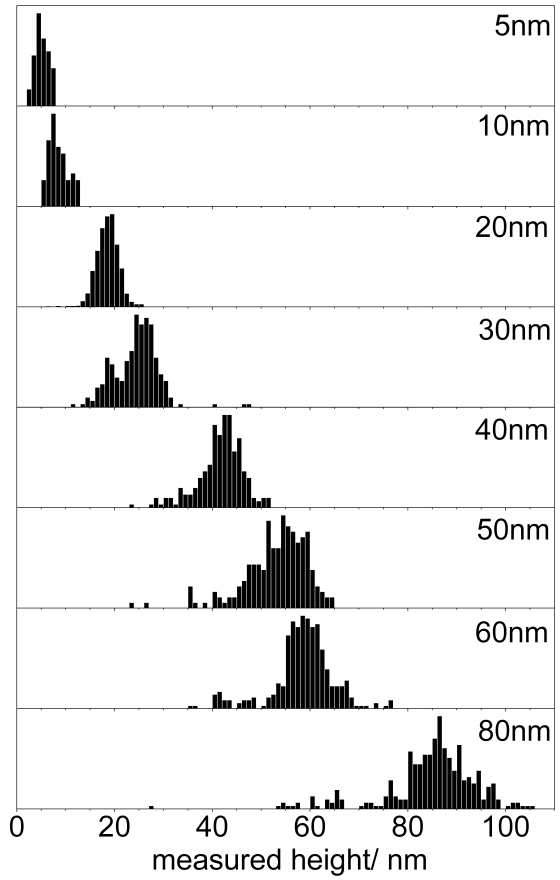

Figure 4.1: Distribution of the heights of commercial spherical gold NPs measured by AFM on APTES-modified glass surfaces. The NPs were imaged in tapping mode in air.

4.3.2 Correlation of AFM and optical microscopy results on gold NPs

To correlate the AFM images with those obtained in optical microscopy, we used a cross as a position reference visible in both types of microscopy techniques. This cross was made by scratching the glass coverslip's surface prior to cleaning and to surface modification. The results of the overlap of images obtained by the scanning-probe and optical absorption microscopy for the sample of 60 nm diameter gold NPs is shown in Fig. 4.2. It is straightforward to find patterns of perfect overlap, enabling unambiguous identification of

the topographical signals of individual nanospheres (white dots in the AFM image) and of their optical absorption signals (red dots). However, the overlap of the two images is not perfect over the whole scanned area due to the hysteresis and to the thermal drift of the AFM scanner during data acquisition time (about 30 min).

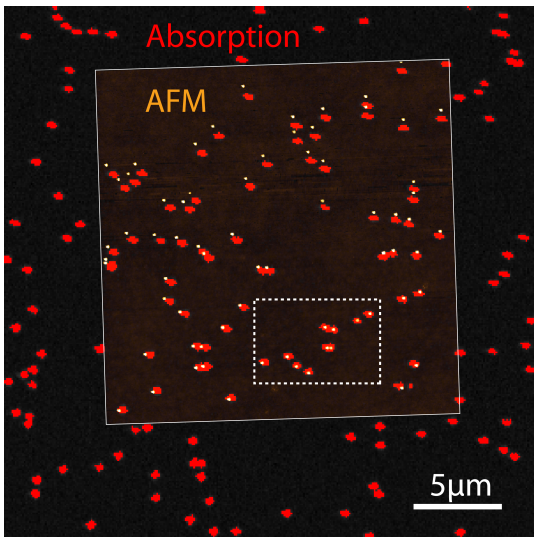

Figure 4.2: Overlap of the optical absorption microscopy image (area 900 μm^2) and of an AFM image (area 400 μm^2 enclosed in solid box) of a sample with 60 nm diameter gold NPs on APTES-modified glass surface. The absorption was measured in glycerol with powers of 29 μW and 2.3 mW for the heating and probe beams, respectively. White dots are individual NPs imaged with AFM and red spots are their optical absorption images. Patterns in NP locations provide an unambiguous correlation between these images. Thermal drift and nonlinearities in the AFM scanner (which has no position feedback) cause a mismatch in the precise location of individual NPs over the whole AFM field. The dashed box highlights an area with good overlap.

4.3.3 Correlation of absorption and luminescence of individual gold NPs

We simultaneously measured absorption (photothermal) and luminescence signals of individual gold NPs (diameters 10, 20, 40, 60, and 80 nm) on an APTES-modified glass surface in glycerol. The AFM and photothermal absorption results are presented in Fig. 4.3 as a scatter plot, where particles of

Table 4.1: Results of the AFM and optical microscopy measurements on commercial gold NPs spin-coated on an APTES-modified glass surface. The height of NPs (H) was measured in tapping mode in air for gold NPs with specified diameters (D). Absorption (photothermal, PTA) and fluorescence microscopy experiments were performed in glycerol, unless specified. The quantum yields (QY) were calculated using results of photothermal microscopy (QY from PTA) and AFM (QY from H).

D [nm]	H [nm]	# NPs	QY from PTA	QY from H	# NPs
5	5.2 ± 1.4	76	$(3.5 \pm 1.4) \times 10^{-7}$	$(3.1 \pm 1.7) \times 10^{-7}$	40 (air)
10	8.5 ± 2	58	$(3.1 \pm 1.2) \times 10^{-7}$	$(3.4 \pm 1.4) \times 10^{-7}$	104
20	18.5 ± 2.3	1811	$(3.7 \pm 1.4) \times 10^{-7}$	$(2.7 \pm 1.4) \times 10^{-7}$	123
			$(1.9 \pm 0.8) \times 10^{-7}$	$(2.2 \pm 1.0) \times 10^{-7}$	107 (air)
30	24.4 ± 4.7	241	–	–	–
40	41.6 ± 4.7	238	$(8.3 \pm 3.3) \times 10^{-7}$	$(3.2 \pm 2.5) \times 10^{-7}$	178
50	53.1 ± 6.6	199	–	–	–
60	58.5 ± 6.4	350	$(9.2 \pm 3.7) \times 10^{-7}$	$(3.0 \pm 2.5) \times 10^{-7}$	218
80	84.7 ± 9.7	323	$(3.3 \pm 2.2) \times 10^{-7}$	$(1.4 \pm 3.9) \times 10^{-7}$	282

different nominal sizes are represented by dots of different colors. As Fig. 4.3 shows, the photothermal signal scales linearly with the volume of NPs deduced from the AFM height. This linear dependence was expected and reported previously.[38,90,95] The linear correlation is well obeyed for particles smaller than 40 nm. We also note a larger spread of photothermal signals for 80 nm NPs. We attribute this spread to a distribution of the local heat transfer parameters (heat conductivities, contact areas) around each individual particle.

Figure 4.4 A presents a scatter plot of luminescence intensity correlated with absorption signal. Particles of different nominal sizes are represented by dots of different colors. The powers of the heating and probe lasers were adjusted in experiments to keep a comparable temperature rise (less than 20 K) at the surface of NPs of different diameters to eliminate laser-induced effects on luminescence (see Section 4.3.4). For all particle sizes, the photothermal signal-to-noise ratio was more than 10 with 3 ms integration time. For luminescence, the signal-to-background ratio was larger than 2 and the signal-to-noise ratio higher than 10. The luminescence signal of smaller NPs (5 nm diameter) was too weak to measure against the fluorescence background of glycerol. Therefore, these particles were measured in air (Fig. 4.4 B), where their luminescence was detected with a signal-to-background ratio of 1 and a

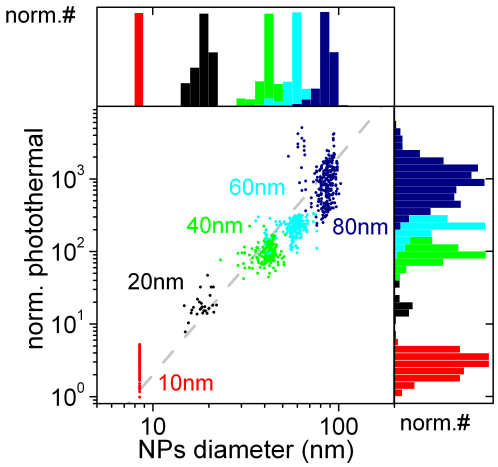

Figure 4.3: Normalized optical absorption (photothermal) signals from gold NPs of different sizes spin-coated on an APTES-modified glass surface in glycerol as a function of their size, as measured by AFM. As we could not correlate AFM with photothermal contrast for 10 nm NPs, we used the average AFM diameter in the plot. The gray line represents a linear relationship between the photothermal signal and NP volume.

signal-to-noise ratio of 5 to 10. The photothermal signal-to-noise ratio of 5 nm diameter NPs in air was more than 10 with 100 ms integration time. The collection efficiencies for the luminescence and photothermal properties differ in air and glycerol. Therefore, we repeated these optical microscopy experiments for a number of 20 nm diameter NPs in air as a reference to calibrate the luminescence and photothermal signal of 5 nm NPs. For these 20 nm NPs, the luminescence signal-to-background ratio was 5, the signal-to-noise ratio was larger than 10, and the photothermal signal-to-noise ratio larger than 30 with 3 ms integration time.

As shown in Fig. 4.4 A, the luminescence roughly scales linearly with the photothermal signal as reported previously by Dulkeith et al.[180] This linear relation is well followed from 5 nm to 20 nm. However, the luminescence signal appears somewhat larger for larger diameters and tends to decrease for very large particles, 80 nm and above. The scaling of the luminescence signal with the volume of the particles instead of their surface area indicates that this luminescence does not arise from surface states or from impurities at the NP's surface and supports the mechanism of particle plasmon emission pro-

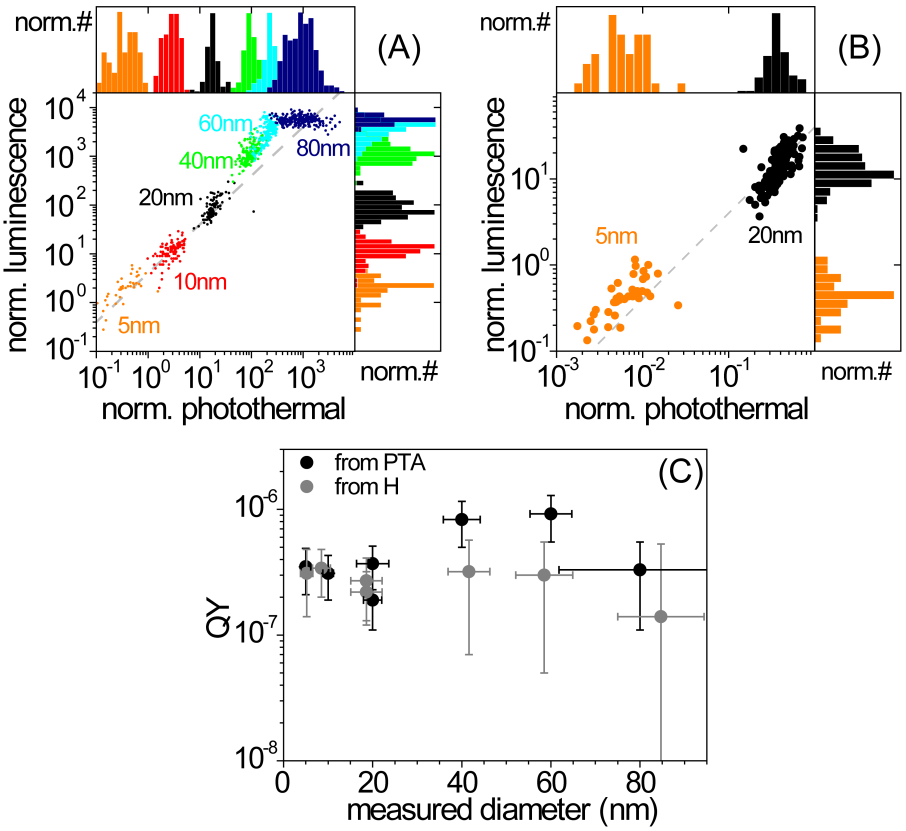

Figure 4.4: A) Combined normalized luminescence and absorption (photothermal) signals from gold NPs of different sizes spin-coated on an APTES-modified glass surface in glycerol. Gray lines [here and in (B)] represent linear relationships between optical signal and NPs volume. B) Normalized luminescence and absorption (photothermal) signals from gold NPs of 5 and 20 nm diameters spin-coated on APTES-modified glass surface in air. Dots represent values for individual NPs. The histograms of signals are shown in the top and right-side axes, correspondingly. C) Luminescence quantum yield (QY) as a function of measured diameters of gold NPs. Estimation of the QY is either based on absorption measurements of size of NPs via photothermal contrast (black dots), or on the size of NPs measured by AFM (gray dots). Error bars in QY represent the spread of values for individual NPs. Error bars for NPs diameters for black and gray dots are defined by the spread of diameters estimated from photothermal microscopy experiments and measured in AFM experiments, respectively

posed by Dulkeith et al.[180] Thus, this luminescence is different from the laser-induced luminescence,[155] which we may attribute to impurities produced at the particle surface by (photo-)chemical reactions (see Section 4.3.4). Furthermore, the good agreement of measurements for 5 nm and 20 nm particles in glycerol and in air is also consistent with a luminescence mechanism involving volume instead of surface states. The signals of 80 nm diameter NPs (Fig. 4.4 A) appear to deviate from the general linear trend of the absorption-luminescence correlation. The luminescence intensity seems to reach a saturation value. This behavior of the luminescence of the largest particles is not clear to us. It may have one or more of the following origins: 1) The nonspherical, ellipsoidal shapes of NPs influence spectrum and magnitude of their absorption and luminescence. Whereas these effects appear to average out for the smaller particles, they may bias the distribution for the larger particles. 2) Large NPs cannot be described within the dipole approximation any more. Multipolar terms can lead to deviations from the simple linear luminescence-absorption scaling. For example, reabsorption of plasmon radiation in the core of large particles could reduce their luminescence yield. 3) Larger particles may have specific defects, facets, or impurities which may modify their luminescence yield with respect to smaller particles.[192]

The luminescence quantum yield (QY) from individual NPs is calculated taking into account the excitation (heating) laser power, luminescence signal, the absorption cross section of a NP, and the detection efficiency, estimated to 5% for our setup. A more accurate measurement of the luminescence detection efficiency of the setup could lead to small changes of the quantum yield (see Appendix C). The absorption cross section in turn is estimated in two ways based on: 1) the absorption (photothermal) signal of NPs which is proportional to the volume in the approximation of Mie scattering,[42] or 2) the height of NPs measured in AFM experiments, which gives the diameter of NPs, assuming a perfect spherical shape. The particles in the optical scans which were outside the AFM scans were also included in the plots, but were assigned the average height measured by AFM. The results of the estimation of QY are shown in Fig. 4.4 C and in Table 4.1. The luminescence QY is found to be almost independent of the size of NPs and estimated to be a few 10^{-7}, in fair agreement with values reported previously.[180] Note that the quantum yields deduced from photothermal values and from AFM values are slightly different for particles larger than 40 nm.

4.3.4 Laser-induced enhancement of luminescence from gold nanospheres

In previous sections of this chapter (Sections 4.3.2 and 4.3.3), we study the intrinsic luminescence of spherical gold nanospheres with sizes ranging from 5 to 80 nm in diameter. In this section, we describe a simple laser-induced method to make 20 nm diameter gold nanospheres more luminescent. Our method relies on the excitation of nanopsheres on an individual basis with a focused laser beam at high powers. In the following, we provide a detailed description of the method, quantify the effect and briefly comment on possible mechanisms that may be responsible for the observed enhancement.

The results of enhancement of gold nanosphere's luminescence are shown in Fig. 4.5 A-I. Time-marks next to each row of images indicate the time since the start of the experiment. Three single 20 nm diameter gold NPs are observed in Fig. 4.5 A, situated more than 500 nm apart. The photothermal signal-to-noise ratios are higher than 300 with 0.26 mW heating power (532 nm) and 40 mW probe power (790 nm) at the sample, and integration time (Δt) of 1 ms. The corresponding temperature elevation at the NP surface caused by the heating light is about 23 K. The absorption of the probe light provides an additional non-modulated temperature rise of 9 K. The full-width-at-half-maximum (FWHM) of the Gaussian fit of the shape of photothermal signal are 220 nm and 260 nm (for vertical and horizontal directions, respectively). The simultaneously acquired confocal luminescence image (Fig. 4.5 B) shows only the background signal in glycerol. The vertical lines observed in the luminescence image (along the fast scan axis) are due to diffusing fluorescent impurities in glycerol. The overlap of the simultaneously detected photothermal Fig. 4.5 A and luminescence Fig. 4.5 B signal is shown in Fig. 4.5 C with the red and green color representing the photothermal and luminescence signal, respectively. The intrinsic photoluminescence signals of 20 nm diameter spheres were not visible in this experiment because of the high fluorescence background signal of the batch of glycerol which was used as immersion liquid.

As a next step, we focus laser beams on the central NP and perform an experiment similar to the one depicted in Fig. 4.6. The graph shows simultaneously recorded photothermal (red) and luminescence (green) time-traces normalized to the heating power. The top part of the graph illustrates how

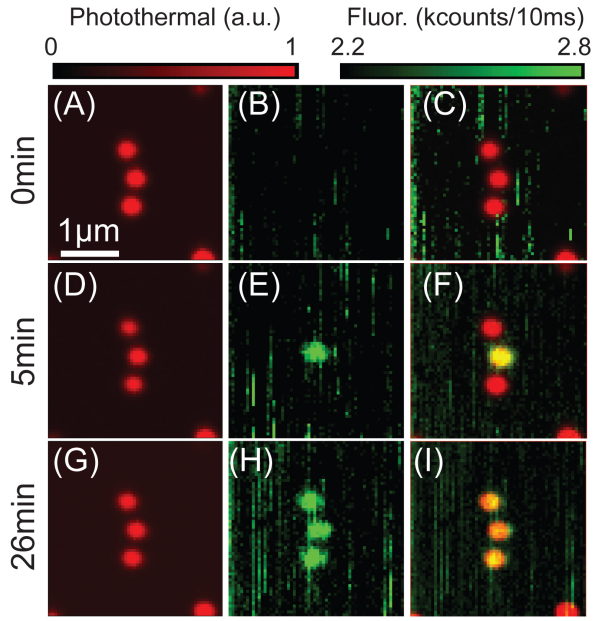

Figure 4.5: Photothermal (A, D, G) and corresponding luminescence (B, E, H) raster scan images simultaneously obtained on 20 nm diameter gold NPs on glass surface in glycerol. (C, F, I) shows the overlap of the two signals. Time-marks next to each row indicate the time since the start of the experiment. Vertical lines (along fast scan axis) in luminescence images originate from diffusing fluorescent impurities in glycerol. There is no detectable luminescence observed from single NPs in (B), while (E) demonstrates bright luminescence from the treated central NP (Fig. 4.6) and others remain non-fluorescent. Finally all three nanospheres have been made fluorescent, as shown in (H). Experimental parameters for raster scans are $P_{heat} = 0.26$ mW and $P_{probe} = 40$ mW at the sample, $\Delta t = 1$ ms, ΔT_{surf} due to heating light (532 nm) is about 23 K.

the heating power is varied in the experiment. The temperature rise on the surface of the nanospheres (ΔT_{surf}) and the photothermal signal depend linearly on the heating power. At approximately 98 s, the heating power has been increased and, with it, the temperature of the NP. The increase of the heating power (514 nm) from 0.26 mW up to 0.85 mW leads to a temperature rise from 17 K up to 57 K on the surface of the NP. At the same time a dramatic increase of the luminescence signal is observed, as well as luminescence fluctuations. The high luminescence signal remains after the heating power is reduced back to 0.26 mW.

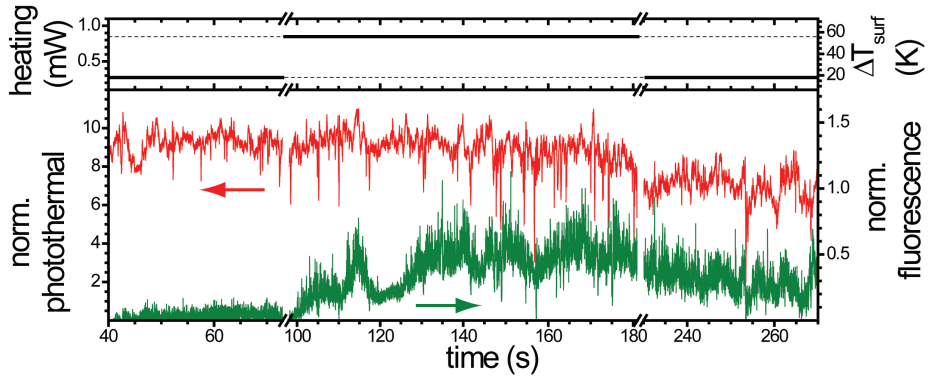

Figure 4.6: A time trace illustrating the appearance of the luminescence signal from a single 20 nm gold NP. An increase of the heating power (top, black) at the first axis break (98 s) leads to the temperature rise at the NP. A significant change in luminescence signal and its fluctuations are observed at the same time (green). At the second axis break (182 s) the heating power is reduced to its starting value. The normalized luminescence signal remains above its background level at the start. Due to the mechanical drift in the setup (about 20 nm min^{-1}) the photothermal signal (red) is about 20% smaller after 230 s. The wavelength of the heating light is 514 nm.

It is important to note that simultaneous photothermal and luminescence raster scans reveal no change in the photothermal signal (Fig. 4.5 D). The unaltered absorption of light suggests no fragmentation of the particle has occurred. A fragmentation of similar size NPs is previously reported with the intense pulsed laser light, where the temperatures rise above 1000 K.[193] We use moderate heating with CW lasers with an order of magnitude lower temperature elevation (less than 100 K) at the surface of NPs. The absence of NPs fragmentation is supported in independent experiments by SEM imaging after the studies of the vibrations of individual gold NPs, where temperature elevation about 300 K is used.[176,194] In contrast to the unchanged absorption, the confocal luminescence image (Fig. 4.5 E) shows a clear change. A fluorescent spot appears with a signal-to-background ratio of 1.4, signal-to-noise ratio of more than 50, and a full width at half-maximum (FWHM) of 300 and 340 nm (for vertical and horizontal directions correspondingly). The spatial overlap of the two images is shown in Fig. 4.5 F with the yellow colour encoding the overlap of photothermal and luminescence signals. The same effect is observed on other NPs in the sample (about 50 NPs tried) and further demonstrated in Fig. 4.5 G, H, I, where the other two NPs in the

image are made fluorescent in the same manner as the middle one. The obtained luminescence persists under illumination for a long time (tested up to 10 min), although its intensity fluctuates. In the particular experiment presented in Fig. 4.5 luminescence was also detected as particles were revisited after 148 min.

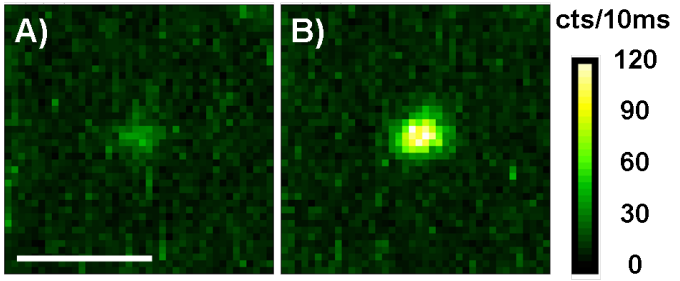

Figure 4.7: Luminescence images of the same 20 nm diameter gold nanosphere A) before and B) after employing the laser-induced treatment of the nanosphere to enhance its luminescence. The excitation power is $P_{heat} = 0.26$ mW at 514 nm. The color scale shows the luminescence count-rate and is the same for both images. The scale bar is 1 μm.

To further quantify the enhancement of the luminescence by the laser-induced method, we repeated the above described experiment on the setup we used to record luminescence images of gold nanoparticles by their intrinsic luminescence (see section 4.3.3). Figure 4.7 shows the luminescence images of the same 20 nm diameter nanosphere. Fig. 4.7 A shows the intrinsic luminescence of the nanosphere, whereas Fig. 4.7 B corresponds to the signal of the same nanosphere after it was treated in the same way as for the nanosphere of Fig. 4.6. The luminescence signal of the nanosphere, under the same excitation and detection conditions, is increased from about 30 cts/10 ms to 110 cts/10 ms by employing the laser-induced luminescence enhancement method. We observe an increase in the luminescence of the nanosphere by a factor of 3 to 4 times. This enhancement factor was confirmed by repeating this measurement on several tens of 20 nm diameter gold spheres.

The enhancement of luminescence upon illumination with laser can be explained by the modification of the surface of NPs, caused by thermal processes, photochemical processes,[195–197] or a combination of those. A temperature-mediated part of the observed enhancement mechanism is sup-

ported by our observation of the enhancement of luminescence after an exposure to only the probe light with a power larger than 150 mW at the sample. In contrast, no enhancement was seen with heating light power kept as low as 0.26 mW for times longer than 200 s, or with the probe light only with powers below 100 mW for times longer than 100 s. However, both observations can not directly exclude a possible effect of the laser illumination on the observed enhancement. We also observe luminescence appearance in pentane and hexane, organic solvents that are chemically different from glycerol. This luminescence enhancement effect is not observed in water, although enhanced luminescence of gold NPs in glycerol remain when glycerol is exchanged with water. The simplest temperature-activated chemical reactions in the above-mentioned solvents would first lead to saturated and therefore non-fluorescent products. A high enough temperature elevation at the surface of NPs, however, can result in the formation of more and more complex unsaturated products, which may decorate the NP and generate luminescence. Still, in order to eliminate the effect of laser light on the observed enhancement, a separate experiment where nanospheres were kept in a heat bath to increase their surface temperature by about 40 degrees should be performed. However, localized excitation and ensemble (macro) heating would be different. An additional complication is the possible catalytic role of the gold surface, which may act in more specific ways than just a local "frying pan".[198–200] Hereafter, we speculate about possible surface chemistry on NPs in glycerol, which requires further investigation: (i) thermal decomposition of glycerol or residual fatty acids in glycerol *, (ii) formation of a reactive acrylic acid aldehyde (acrolein, $H_2C = CH - CHO$ obtained in thermal decomposition of glycerol by dehydration in the presence of a catalyst . Recently, reversible and irreversible temperature mediated reactions of glycerol and citric acid[201] have been studied with the method of differential scanning calorimetry (DSC) in the temperature range of $20 - 220^{\circ}C$. The work reports irreversible esterification and glycerol citrate polyesters formation. Also, Ruppert et al.[202] have studied a selective etherification of glycerol to linear, branched and cyclic diglycerols, and triglycerol in the presence of alkaline earth metal oxides.

*Communication with Sigma-Aldrich

4.4 Conclusions

Herein, we have correlated three observation methods (AFM topography, optical photothermal absorption, and optical photoluminescence) on individual gold nanospheres of different sizes, from 5 to 80 nm. The AFM height signal gives a very good indication of the particle's volume, as deduced from absorption properties, at least for large enough particles. Photothermal detection is much easier than AFM for small particles (5 nm and lower), particularly when those have to be found over large sample areas.

Our measurements confirm that the photoluminescence signal scales roughly as the volume of the NPs, and that the luminescence yield is therefore roughly independent of size, from 5 to 60 nm. The value of the yield is about 3×10^{-7} (subject to a possible small calibration error, see Appendix C), in good agreement with previous determinations. We also find that the yield appears to decrease for even larger particles (larger than 80 nm in diameter).

We also demonstrate a simple method to make commercial 20 nm diameter gold NPs more luminescent. The luminescence enhancement appears after the laser excitation of the NPs at moderately high power, which leads to a transient temperature elevation at the surface of NPs and modification of their surface properties. We observe this effect in different solvents (glycerol, hexane, pentane). We shortly speculate on the origin of the observed enhancement in order to stimulate research and we suggest that temperature-assisted (photo-)chemical reactions lead to a complex modification of the surface of gold NPs. However, the mechanism which is responsible for the laser-induced enhancement of luminescence still remains a subject to study. In order to identify and separate between different mechanism, more rigorous studies (e.g. Raman spectroscopy or two-photon excited photothermal microscopy) at single-particle level are required to find the effect of NP's size, surface modification and environment on the observed enhancement.[131].

Independently of AFM measurements, the combined optical absorption and luminescence microscopy of individual NPs is a convenient new method to study luminescence of gold particles with various shapes and to compare to theory. Gold nanorods, platelets, stars, cubes, pyramids, and various organic or hybrid NPs are obvious candidates for future investigations. Absorption and luminescence properties of these NPs can be used for applications where the combination of photostability and brightness of the labels are

required.

Acknowledgements

We thank Dr. Peter Zijlstra for helpful discussions of the origins of gold NPs luminescence, as well as the BioAFM Lab at Leiden Institute of Physics, in particular Dr. Federica Galli and Prof. Tjerk Oosterkamp for the support with AFM equipment. We acknowledge the financial support by ERC (Advanced Grant SiMoSoMa).